First-principles calculation of the electronic structure of sapphire: Bulk states

J. Guo, D. E. Ellis, and D. J. Lam
Materials Science Division, Argonne National Laboratory, Argonne, Illinois 60439
(Received 8 April 1991; revised manuscript received 19 September 1991)

The electronic structure of sapphire, α–Al_2O_3, was calculated using the self-consistent-field discrete variational method in the local-density framework. Clusters of the size of 26–80 atoms embedded in the infinite host lattice were used to model the sapphire single crystal. A three-dimensional Ewald summation was used to obtain the Coulomb potential of the infinite lattice. Calculations were performed on ten clusters centered at four points of different point-group symmetries in bulk sapphire. The consistency of the calculated electronic structure among these ten clusters and good agreement with experimental data and recent first-principles band-structure calculations indicate that the bulk values can be achieved with clusters of modest size. Features in the valence density of states are interpreted with the help of the bond densities between the O atom and its near neighbors. Bulk sapphire is found to be mostly ionic measured by about 2% orbital overlaps between nearest-neighbor Al and O atoms, with no charge accumulation in the bonding region.

I. INTRODUCTION

The self-consistent field (SCF) embedded-cluster method is a useful scheme for studying electronic structure and energetics of complex oxide systems, containing substituent ions and defects.[1–5] However, the cluster size and boundary conditions are always problematic. Recently, improvements in cluster calculations have resulted from advances in the embedding scheme and more ample choices of cluster sizes and shapes.[6] Because of the availability of experimental data and recent first-principles SCF band-structure calculations,[7] we used α–Al_2O_3 to test our embedded-cluster method with the objective of extending it to study more difficult problems, e.g., defects, crystal surfaces, and substitutions in oxide systems, which are not readily done by band methods. The goal of the present paper is to establish the size of clusters needed and the level of accuracy obtainable within the embedded-cluster model, using the self-consistent charge scheme and the concept of *seed atoms*.

Electronic structure of bulk Al_2O_3 has been extensively studied by many experimental techniques such as vacuum ultraviolet spectroscopy (VUS),[8] x-ray-absorption spectroscopy (XAS),[9–14] x-ray-emission spectroscopy (XES),[9,14–17] x-ray photoemission spectroscopy (XPS),[18,19] and electron energy-loss spectroscopy (EELS).[20]

The early self-consistent-field (SCF) Xα scattered-wave calculations using a model $[AlO_6]^{9-}$ octahedral cluster[21] failed to give the total width of the occupied and unoccupied states obtained from XAS (Ref. 14) and XPS.[18,19] Later band-structure calculations based on the semiempirical Mulliken-Rudenberg method,[22] the tight-binding method,[23] and the extended Huckel method[24] appeared to be in better agreement with experimental data. However, due to the lack of self-consistency and the usage of several adjustable parameters, the calculated results from these methods sensitively depend on the parameters which were usually fitted from some experimental data.

Using the self-consistent local-density embedded-cluster method, Xia *et al.*[3] have calculated the electronic structure of sapphire and its Cr substituted defected structure ruby (Al_2O_3:Cr^{3+}). Recently, Xu and Ching[7] have performed first-principles SCF band-structure calculations using the orthogonalized linear combinations of atomic orbitals method. The optical properties obtained from their calculations compared favorably with experiment.[8]

This paper is divided into four sections. The next section gives a review of the discrete variational embedded-cluster method, and definitions of physical quantities present in the paper. Section III presents the self-consistent results calculated from ten clusters centered at four points of different point-group symmetry in the bulk sapphire lattice. Comparisons are made with experimental data and other theoretical band-structure calculations. Section IV gives our conclusions.

II. THEORETICAL APPROACH

A. Crystal structure and clusters chosen

The atomic structure of sapphire, α–Al_2O_3, is typified by that of chromium sesquioxide, Cr_2O_3.[25] It has a rhombohedral symmetry with two molecules in the primitive cell. The space group is D^6_{3d}. The corresponding hexagonal unit cell, a larger cell containing 12 Al and 18 O atoms, is shown in Fig. 1 with $a = 4.76$ Å and $c = 13.00$ Å.[25] The cell shown in Fig. 1 has the S_6 point-group symmetry with respect to its center. There are only two chemically distinct atoms, i.e., Al and O atoms. Their near-neighbor atom coordinations are listed in Tables I and II and drawn in Figs. 2(a) and 2(b).

In the embedded-cluster method, the cluster of minimum size should contain the two chemically distinct Al and O atoms and their nearest-neighboring atoms. For

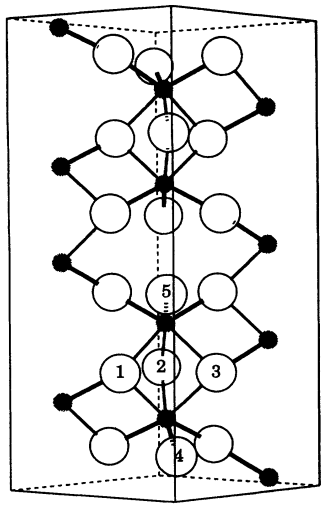

FIG. 1. A perspective view of the hexagonal unit cell of sapphire. The filled circles label Al atoms, and open circles O atoms. The dark thick lines label the short Al-O bonds (1.86 Å), the light thin lines the long Al-O bonds (1.97 Å).

clusters of such size, there exist certain Al and O atoms which are *chemically complete* in the sense that all atoms to which they are bonded are also contained within the cluster variational space. We call these chemically complete Al and O atoms the *seed* atoms, and they will serve to determine the self-consistent potential. To investigate the effect of the choices of the cluster center on the calculated results, we select the four sites of different point-group symmetry on the bulk crystal. These four sites are (a) O atom site of C_2 symmetry, (b) Al atom site of C_3 symmetry, (c) the inversion center of S_6 symmetry, which is the center of Fig. 1, and (d) the center of the triangle formed by three O atoms labeled as 1,2,3 in Fig. 1 of D_3 symmetry. Atoms within the spheres centered at these four sites and of 4 Å radius were chosen as the cluster atoms, and the remaining atoms were treated as *host* atoms. Host atoms enter into formations of the total charge density and potential, but are not part of the cluster variational space. Due to the low symmetry of the site (a), we chose a smaller cutoff radius of 3.8 Å, i.e., two Al atoms and O atoms from the cluster were switched into the host. Shown in Fig. 2 are the perspective views of these four clusters.

To investigate how cluster size affects the calculated results and to check the convergence of calculated results, we performed calculations on the following larger clusters: 48 and 60 atoms with radii 4.5 Å and 5.1 Å centered at site (b), 44-atom with 4.5 Å radius centered at site (c), and 38, 62, and 80 atoms with radii 4.4 Å, 4.9 Å, and 5.5 Å centered at site (d).

TABLE I. The near-neighbor atom coordinations of O atom.

Atom type	Label[a]	Number of atom	Distance (Å)
Al	2	2	1.86
	3	2	1.97
	8	2	3.22
O	4	2	2.52
	5	2	2.61
	6	4	2.73
	7	4	2.87
	11	4	3.79

[a]Same as the labels shown in Fig. 2(a).

B. Solving the local-density equation

The self-consistent local-density discrete variational method has been used to study the electronic structure of free molecules and clusters[26–28] for about two decades. Its extension into the studies of infinite (bulk) systems has proceeded over the past several years.[6,29–32]

Using a variational approach with symmetrized basis functions localized within the region of the cluster, we solve the local-density Schrödinger equation

$$H\Psi_i = \varepsilon_i \Psi_i \ , \tag{1}$$

where $H = T + V^c + V_{xc}$ is the three-dimensional periodic Hamiltonian and ε_i, Ψ_i are the energy and wave function of the ith molecular orbital. The wave functions are given as

$$\Psi_i^{\Gamma} = \sum_{\nu n l \gamma} C^i_{\Gamma \nu n l \gamma} \Phi^{\Gamma\gamma}_{\nu n l} \ , \tag{2}$$

or in abbreviated form

$$\Psi_i = \sum_k C^i_k \Phi_k, \quad k = \{\Gamma, \nu, n, l, \gamma\} \ , \tag{3}$$

where $\Phi^{\Gamma\gamma}_{\nu n l}$ is the symmetrized basis function builtup from atoms of type ν with the principal quantum number n, angular quantum number l. The irreducible representation Γ and the partner γ completely specify the orbital symmetry under point group operations. By multiplying with basis function Φ_j on both sides of Eq. (1) and then integrating over real space, we have

$$\sum_k H_{jk} C^i_k = \varepsilon_i \sum_k S_{jk} C^i_k \tag{4}$$

TABLE II. The near-neighbor atom coordinations of Al atom.

Atom type	Label[a]	Number of atom	Distance (Å)
O	2	3	1.86
	3	3	1.97
	7	3	3.22
Al	4	1	2.65
	5	3	2.79
	6	3	3.22

[a]Same as the labels shown in Fig. 2(b).

or

$$(S^{-1}H - \varepsilon_i I)C^i = 0 \,, \tag{5}$$

where $H_{jk} = \langle\Phi_j|H|\Phi_k\rangle, S_{jk} = \langle\Phi_j|\Phi_k\rangle$ are evaluated using a quasirandom numerical integration scheme.[33–35] By diagonalizing the above matrix, we obtain the eigenvalues $\{\varepsilon_i\}$ and eigenvectors $\{C^i_k\}$.

C. Construction of basis functions

The symmetrized basis functions $\Phi^{\Gamma\gamma}_{\nu nl}$ were obtained as

$$\Phi^{\Gamma\gamma}_{\nu nl}(\mathbf{r}) = \sum_{mj} A^{\Gamma\gamma}_{\nu lmj} R_{\nu nl}(r_{\nu j}) Y_{lm}(\hat{r}_{\nu j}) \,, \tag{6}$$

$$\mathbf{r}_{\nu j} = \mathbf{r} - \boldsymbol{\tau}_{\nu j} \,,$$

where $A^{\Gamma\gamma}_{\nu lmj}$ is the symmetry coefficient, $R_{\nu nl}(r_{\nu j})$ is the radial wave function with principal quantum number n and angular quantum number l centered at the jth atomic site of type ν, and Y_{lm} is the spherical harmonic function. The radial wave functions can be obtained in the following two ways.

(1) The self-consistent local-density solutions of the corresponding atoms with appropriate electron occupation numbers $n_{\nu nl}$.

(2) The numerical solutions of a potential spherically averaged from the cluster potential.

In both cases, a potential well or parabolic matching potential are used to localize the wave functions. For all the calculations presented here the first kind of basis was adopted, with the occupation numbers $n_{\nu nl}$ updated to the corresponding self-consistent Mulliken populations obtained from the embedded-cluster calculations.

D. Construction of potentials

In order to construct the potential, we first need to know the charge density. The charge density associated

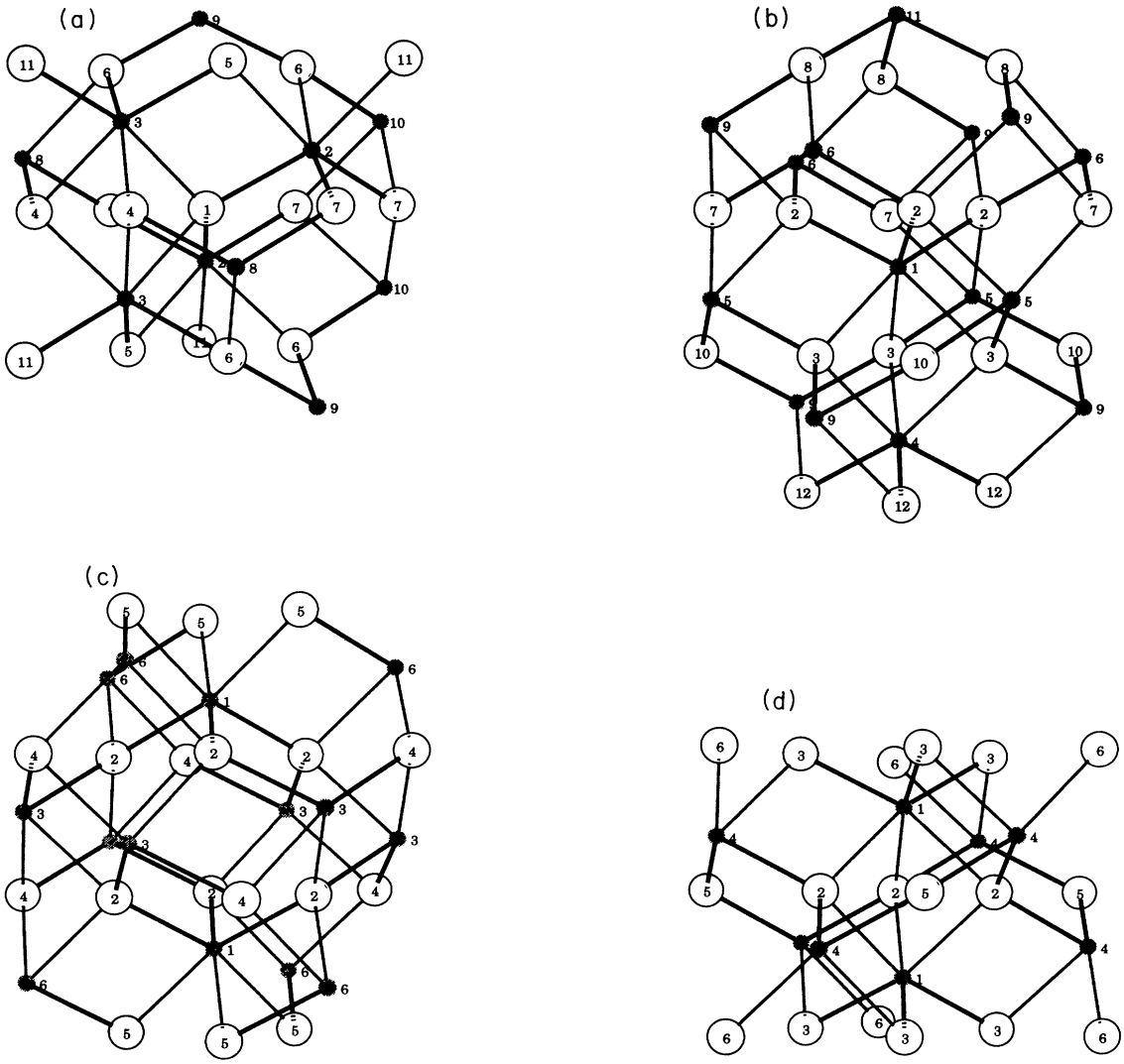

FIG. 2. Perspective views of the four clusters chosen in the calculations. (a) 27-atom cluster of C_2 symmetry; (b) 33-atom cluster of C_3 symmetry; (c) 32-atom cluster of S_6 symmetry; (d) 26-atom cluster of D_3 symmetry. The numbers label the different shells of atoms in the ascending order according to their distances from the center. Same conventions as Fig. 1.

with atomic site ν in the spherical charge approximation is given by

$$\rho_\nu(\mathbf{r}) = \sum_{nl} n_{\nu nl} |R_{\nu nl}(r)|^2 , \tag{7}$$

where $n_{\nu nl}$ is the electron occupation number to be determined self-consistently. The charge density of the bulk material is the lattice summation of ρ_ν of the seed atoms given as

$$\rho(\mathbf{r}) = \sum_{\mu=1}^{\infty} \sum_{\nu=1}^{N} \rho_\nu(r_{\nu\mu}) ,$$
$$\mathbf{r}_{\nu\mu} = \mathbf{r} - \boldsymbol{\tau}_\nu - \mathbf{R}_\mu , \tag{8}$$

where N is total number of atoms in the unit cell, $\mathbf{r}_\nu$ the nuclear position, and $\mathbf{R}_\mu$ is a lattice vector.

The Coulomb potential V^c is constructed as

$$V^c(\mathbf{r}) = \sum_{\mu=1}^{\infty} \sum_{\nu=1}^{N} V_\nu^c(r_{\nu\mu}) , \tag{9}$$

where V_ν^c is the Coulomb potential associated with charge density ρ_ν. For the oxide materials studied, in general we have ionic charges

$$Q_\nu = \int \rho_\nu \, d^3r, \quad \lim_{r\to\infty} V_\nu^c = \frac{Q_\nu}{r} . \tag{10}$$

Therefore, the summation in Eq. (9) converges very slowly. One generally used an efficient summation scheme of Ewald[36,37] which introduces a Gaussian charge density associated with site ν as

$$\rho_\nu(\mathbf{r}) = \frac{Q_\nu}{(\sqrt{\pi}a)^3} e^{-r^2/a^2} , \tag{11}$$

where a is the width parameter to be chosen later to achieve fast convergence. The corresponding Coulomb potential is

$$V_\nu^G(\mathbf{r}) = \frac{Q_\nu}{r} \mathrm{erf}\left(\frac{r}{a}\right), \quad \lim_{r\to\infty} V_\nu^G = \frac{Q_\nu}{r} , \tag{12}$$

where erf(r) is the error function. The total Coulomb potential from these Gaussian charges can be evaluated in k space as

$$V^G(\mathbf{r}) = \frac{4\pi}{\Delta} \sum_{\tau=1}^{\infty} \sum_{\nu=1}^{N} \frac{Q_\nu}{K_\tau^2} \exp\left(i\mathbf{K}_\tau \cdot (\mathbf{r} - \mathbf{r}_\nu) - \frac{(K_\tau a)^2}{4} \right) , \tag{13}$$

where Δ is the volume of the crystal unit cell. The width a can be chosen for rapid convergence of both the real and k space summations.

In the local-density approximation, the exchange and correlation potential V_{xc} only depends on the local charge density ρ. Among several different expressions of V_{xc},[38–41] we chose the simple form given as

$$V_{\mathrm{xc}} = -\alpha \frac{3}{2} \left(\frac{3}{\pi}\right)^{1/3} \rho^{1/3} , \tag{14}$$

with $\alpha = 0.7$ in all of our calculations. This is in the same form as the $X\alpha$ method proposed by Slater,[42] with an α value consistent with many-body theory and experimental comparisons.

In more recent electronic structure and total-energy calculations of atoms, molecules, and metals, nonlocal corrections in the exchange-correlation potential have been made to obtain better agreements between theory and experiment.[43–49] Application of nonlocal potential in a large embedded-cluster calculation has not been explored at the present time.

Because only the basis functions (electrons) associated with the cluster atoms enter the variational calculation, the deep core potentials on host atoms close to cluster atoms will try to pull the electrons of the cluster into them. This attraction is counterbalanced by the electrons of the host atoms through the Pauli exclusion principle. The electrons of the cluster should finally avoid these exterior atom regions. Consistent with pseudopotential arguments, we truncated the deep core potentials to a constant, set at the Fermi level within a certain radius (usually $\sim$ 2 a.u.). Varying the radius or well depth of the exterior atom core pseudopotential over a reasonable range has very little effect on calculated properties.

E. Evaluations of charge density and various properties

The electrons of the cluster are filled successively into the cluster orbitals Ψ_i according to the Fermi-Dirac statistics as

$$n_i = \frac{1}{e^{(\varepsilon_i - \varepsilon_F)/k_B T} + 1} , \tag{15}$$

where n_i is the occupation number, ε_F the Fermi energy, k_B the Boltzmann constant, and T the temperature set to be zero in our calculations here. The question now is how to assign the total number of electrons for the cluster chosen. The answer is trivial if the cluster happens to contain an integer number of bulk unit cells, i.e., it is a neutral cluster. However, clusters chosen in Sec. II A usually do not fall into this category. The charge of the cluster is generally not known beforehand since nonintegral charges Q_ν are obtained.

We determine the Fermi energy ε_F and the total number of electrons in the cluster N_{cluster} using the following procedures, which guarantee a stoichiometric crystal model potential. First we approximate the full charge matrix by a diagonal matrix similar to the scheme proposed by Mulliken[50] as

$$N_{\mathrm{cluster}} = \sum_{i=1}^{\mathrm{occ}} n_i = \sum_j N_j ,$$
$$N_j = \sum_k \frac{2N_{jj}N_{jk}}{N_{jj} + N_{kk}} , \tag{16}$$

where n_i is given in Eq. (15), and N_{jk} given as

$$N_{jk} = \sum_{i=1}^{\text{occ}} n_i C_j^i C_k^i S_{jk} \ . \tag{17}$$

The N_j are thus effective occupation numbers of the basis orbitals. For n_μ seed atoms of type μ in the cluster, there exists a unique value of β_μ such that $\beta_\mu n_\mu$ equal to the number of atoms of type μ in the unit cell. The neutrality of the unit cell requires that

$$\sum_\mu \beta_\mu n_\mu N_\mu = \sum_\mu \beta_\mu n_\mu Z_\mu \ , \tag{18}$$

where the summation is over the number of seed atom types, Z_μ is the atomic number, and N_μ given as

$$N_\mu = \sum_{nl\Gamma\gamma} N_j, \ \ j = \{\mu, n, l, \Gamma, \gamma\} \ . \tag{19}$$

From Eqs. (15) and (16)–(19), the Fermi energy ε_F and occupation number n_i can be uniquely determined. The role of β_μ is to guarantee a stoichiometric (charge neutral) crystal model potential. A similar scheme was proposed by Goodman *et al.* in calculations of electronic structure for copper oxides and high-T_c compounds.[6]

Given the occupation number n_i, the cluster charge density is obtained as

$$\rho_{\text{cluster}}(\mathbf{r}) = \sum_{i=1}^{\text{occ}} n_i |\Psi_i|^2 \ , \tag{20}$$

which can be projected into each atomic site μ according to the weighting scheme given in Eq. (16) as

$$\rho_{\text{cluster}}(\mathbf{r}) = \sum_\nu \rho_\nu(\mathbf{r}'), \ \ \mathbf{r}' = \mathbf{r} - \mathbf{r}_\nu$$
$$\rho_\nu(\mathbf{r}') \approx \sum_{nl} n_{\nu nl} |R_{\nu nl}(r'_\nu)|^2 \ , \tag{21}$$

where $R_{\nu nl}$ is the same as in Eq. (7).

The Mulliken population $n_{\nu nl}$ associated with atomic orbital νnl is given by

$$n_{\nu nl} = \sum_{\Gamma\gamma} N_j, \ \ j = \{\nu, n, l, \Gamma, \gamma\} \tag{22}$$

with N_j defined in Eq. (16). By mixing $n_{\nu nl}$ with the $n_{\nu nl}$ in the previous cycle, we can construct the charge density associated with atomic site ν and using Eq. (8) to obtain the total charge density of the bulk material, where only the ρ_ν associated with the seed atoms are used. This process is reiterated until the $n_{\nu nl}$ converge to a desired degree of precision.

The partial density of states associated with atomic orbital νnl is defined as

$$D_{\nu nl}(\varepsilon) = \sum_i F_{\nu nl}^i L(\varepsilon - \varepsilon_i) \ . \tag{23}$$

Here $F_{\nu nl}^i$ is given as

$$F_{\nu nl}^i = \sum_{\gamma k} C_j^i C_k^i S_{jk} \ , \tag{24}$$

with j as short label for $\{\nu nl\gamma\}$ and C the eigenvector, and S_{jk} the overlap matrix element. L is the Lorentzian line shape

$$L(\varepsilon) = \frac{\gamma/\pi}{\varepsilon^2 + \gamma^2} \ , \tag{25}$$

with γ the half-width set to 0.5 eV in the present paper.

The bond density between two atomic orbitals νnl and $\nu' n' l'$ is defined as

$$B_{\nu' n' l'}^{\nu nl}(\varepsilon) = \sum_i \sum_{\gamma\gamma'} C_j^i C_k^i S_{jk} L(\varepsilon - \varepsilon_i) \ , \tag{26}$$

where j and k are short labels for $\{\nu nl\Gamma\gamma\}$ and $\{\nu' n' l'\Gamma\gamma'\}$. The bond density measures the energy distribution of overlap between the two atomic orbitals considered and thus provides a quantitative measure of the covalency in the interaction between these two atoms. Positive bond density means that the overlap of the two atomic orbitals is in phase, and the kinetic energy is lower around the interatomic region, which is a criterion for *bonding orbitals*. On the other hand, negative bond density indicates *antibonding* interactions which in a simple one-electron picture lead to interatomic repulsion.

III. RESULTS

A. Optimized basis functions

In all of electronic structure calculations using variational methods to solve the Schrödinger equation, the flexibility of the basis functions is an important factor in determining the accuracy of the calculated results. We can improve the basis flexibility by the following two schemes.

(1) Increasing the number of the basis functions of a chosen form, e.g., adding further νnlm radial and angular functions.

(2) Keeping the number of basis functions to the minimum and optimizing their shape for the particular system considered.

We adopted the second scheme here, since it preserves the validity of the usual chemical bonding and orbital analyses. The Mulliken orbital populations and effective atomic configurations provide a very useful interpretation of the chemical state of the crystal. Unfortunately, in the first scheme these useful analyses lose their utility due to the diffuse nature of the extended functions. The total charge density and its derived properties should be the same of course, provided both schemes are carried out properly.

We optimized our minimum basis functions for all the calculations presented in this paper as described in Sec. II C. We have checked the uniqueness and convergence of our basis optimization scheme by performing the calculations of the 26-atom cluster centered at site (d) from two extremes. We started our calculations from bases and initial orbital populations of the neutral Al, O atoms and fully ionized Al^{3+}, O^{2-} ions. After achieving the self-consistency, they both arrived at the same configuration with orbital occupations of Al $3s^{0.04}3p^{0.04}$ and

O $2s^{2.00}2p^{5.94}$. Three steps of bases optimization (i.e., $O^{1.1-}$, $O^{1.8-}$, and $O^{1.9-}$ with corresponding charged Al atoms) were required to converge at the final configuration starting from the neutral atoms compared with one step ($O^{1.9-}$) starting from the fully ionized atoms. Thus in the remaining calculations the initial configurations were chosen as the fully ionized atoms.

B. Density of states

Shown in Fig. 3 are partial density of states (PDOS) for O $2s2p$ states and Al $3s3p$ states from the four clusters of similar size, centered at four different sites (a)–(d) as shown in Fig. 2. The plotted Al and O PDOS are from the seed (fully coordinated in the cluster chosen) Al and O atoms, whose charge densities are used in the construction of the three-dimensional periodic potential. The PDOS shown are normalized to one molecular formula unit of α–Al_2O_3 and convoluted by a Lorentzian function of 0.5 eV full width at the half maximum height. The total density of states is the sum of the Al and O PDOS curves. It should be emphasized that the zero of energy scale shown is the vacuum level which was calculated explicitly and no artificial alignment of levels is used here. States below −9 eV are all occupied and the ones above unoccupied.

From Fig. 3, we see that the widths and locations of major features of these four groups of curves are quite similar. The lower valence states, which are mainly made up of the O $2s$ states, have a main peak around −26 eV and a secondary peak or shoulder around −28 eV; the upper valence states, which are mainly made up of the O $2p$ states, have a main peak around −11 eV, two secondary peaks around −15 and −13 eV; the conduction states, which are mainly made up of the Al $3s3p$ states, have a main peak around 8 eV, several secondary peaks from 2 to 5 eV. It indicates that the choices of different cluster centers have little effect on the calculated electronic structure results as long as all the seed atoms are fully coordinated.

To see how fast our embedding scheme converges, we performed further calculations using six larger clusters, the PDOS of which are shown in Fig. 4. From Fig. 4, we see that the features present in the PDOS shown in Fig. 3 are preserved but became broader as the cluster size increases. This is due to the increase in number of molecular orbitals as we increase the size of the cluster. Eventually these discrete molecular levels will become the energy band as the cluster size approaches infinity; it is interesting to see that 60 atoms is sufficient for most spectroscopic comparisons. From Figs. 3 and 4, we see that all the major features in the PDOS appear when the size of the cluster is around 30 atoms, and that their locations and relative intensities converge to the same values regardless of the choices of cluster center when we further increase the size of the cluster. In practice, it saves computation time to use a cluster with high-symmetry site as center if all the seed atoms in the cluster are fully coordinated and the cluster has the smallest number of atoms. Therefore, for sapphire the best cluster is centered at site (d). The 26-atom cluster centered in this site gives all the major features shown in the PDOS of larger clusters. The cluster centered at site (c) of S_6 symmetry is not as good as site (d) of D_3 symmetry. Because this cluster is equivalent to two clusters of site (d) related by an inversion operation, twice the number of atoms is required to achieve the same degree of coordination for

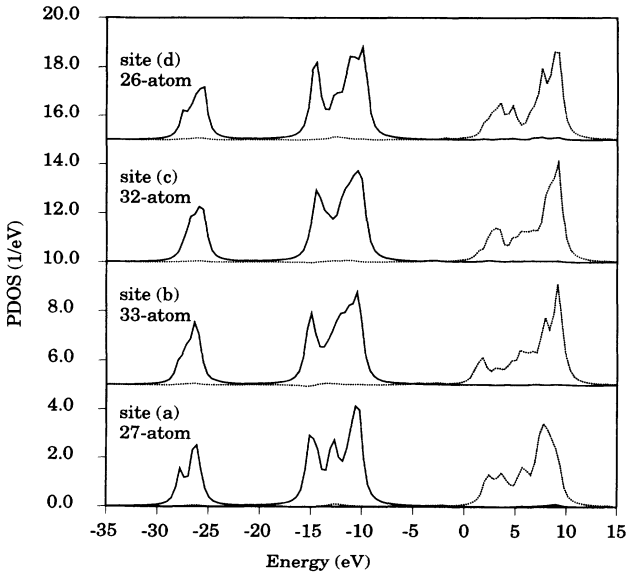

FIG. 3. Partial density of states for O $2s2p$ states (solid curves) and Al $3s3p$ states (dotted curves). The four groups of curves from bottom to top are for the four clusters (a)–(d) shown in Fig. 2 and are shifted upwards for a clear view. The curves are normalized to one molecular formula of α–Al_2O_3. The zeros of energy scales for all curves are the vacuum level, which was calculated explicitly.

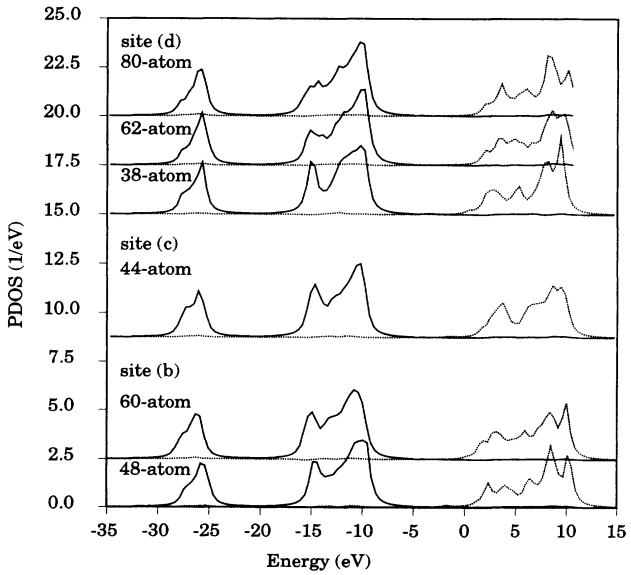

FIG. 4. Partial density of states for O $2s2p$ states (solid curves) and Al $3s3p$ states (dotted curves). The six groups of curves from bottom to top are for the six larger clusters centered at the sites (b) and (c). Same conventions as Fig. 3.

TABLE III. The locations and widths of valence and conduction bands calculated for the ten clusters studied. The data given are in units of eV.

Type	Lower valence band			Upper valence band			Conduction band		
	E_{min}	E_{max}	ΔE	E_{min}	E_{max}	ΔE	E_{min}	E_{max}	ΔE
27 atom	-28.2	-26.2	2.0	-15.6	-10.4	5.2	1.0	9.0	8.0
33 atom	-27.9	-25.9	2.0	-15.5	-10.1	5.4	1.0	9.9	8.9
48 atom	-27.4	-25.2	2.2	-15.1	-9.5	5.6	1.3	10.2	8.9
60 atom	-28.0	-25.7	2.3	-15.7	-9.6	6.1	1.1	10.0	8.9
32 atom	-27.4	-25.4	2.0	-15.0	-9.8	5.4	1.4	9.4	8.0
44 atom	-27.8	-25.4	2.4	-15.3	-9.8	5.4	1.7	10.0	8.3
26 atom	-27.6	-25.6	2.0	-14.6	-9.8	4.8	1.7	9.0	7.3
38 atom	-27.7	-25.6	2.1	-15.5	-9.8	5.7	0.2	9.5	9.3
62 atom	-27.9	-25.5	2.4	-15.8	-9.8	6.0	1.6	10.0	8.4
80 atom	-28.0	-25.6	2.4	-16.0	-9.8	6.2	1.6	10.2	8.6

the seed Al, O atoms. This is demonstrated by the close similarity in the PDOS between the 26-atom cluster centered at site (d) shown in Fig. 3 and the 44-atoms cluster centered at site (c) shown in Fig. 4. We summarize in Table III the positions and widths of the two valence bands and the unoccupied conduction band for the ten clusters studied.

A comparison of our calculated bandwidths and interband gaps with band-structure results and experimental estimates is given in Table IV. We see that our calculated valence DOS compare well with band calculations and experiments. In addition, the relative intensities and locations of major features in our total valence density of states agree well with the recent band-structure calculation.[7] A band within the energy range of 6.3 eV to 10 eV above the top of the valence band found in the band calculation,[7] which gives the 6.3 eV energy gap, is not present in our calculation. This is due to the essential difference of quasilocalized states obtained in the ground-state potential for a cluster model as opposed to a delocalized band model.[3]

C. Bond density

In the rest of this paper we will discuss the results obtained from the 80-atom cluster centered at site (d). Since our basis function optimization scheme mainly optimizes the bases for the occupied valence states, it provides a better description for the ground state. Due to the limited basis functions flexibility for the continuum states above the vacuum level (Al $3d$ and O $3s3p$ states were not included in our bases), our calculated unoccupied states are not as accurate as the valence states.

TABLE IV. Comparison of calculated lower and upper valence bandwidths and interband gaps (eV) of sapphire with experiments.

Type	Width (LVB)	Gap (LVB-UVB)	Width (UVB)	Energy gap
Present work[a]	2.4	9.6	6.2	11.4
OLCAO[b]	3.3	8.5	7.4	6.3
ETB[c]	3.0	10.0	6.0	~8.0
ETH[d]	9.5	6.3	11.8	8.7
Expt[e]			~8.0	
Expt[f]				9.2
Expt[g]	~6.0	~4.0	~15.0	
Expt[h]	~9.0	~6.0		

[a]Data obtained from the converged results of the 80-atom cluster centered at site (d).
[b]First-principles SCF orthogonalized linear combinations of atomic orbitals method.[7]
[c]Extended tight-binding method.[23]
[d]Extended Huckel method.[24]
[e]Polarized x-ray emission.[15]
[f]Vacuum ultraviolet spectroscopy.[8]
[g]X-ray photoemission.[18]
[h]X-ray spectroscopy.[14]

However, as demonstrated in our previous works,[51,52] these calculated unoccupied states above the vacuum level do give some approximate measure of the existence of these Al $3s3p$ states and their relative energy positions, which are accessible by photoelectrons from x-ray near-edge absorptions.

Since in this paper we are mainly interested in the ground-state properties, we plot in Fig. 5 the bond densities of the 80-atom cluster in the valence-band region,

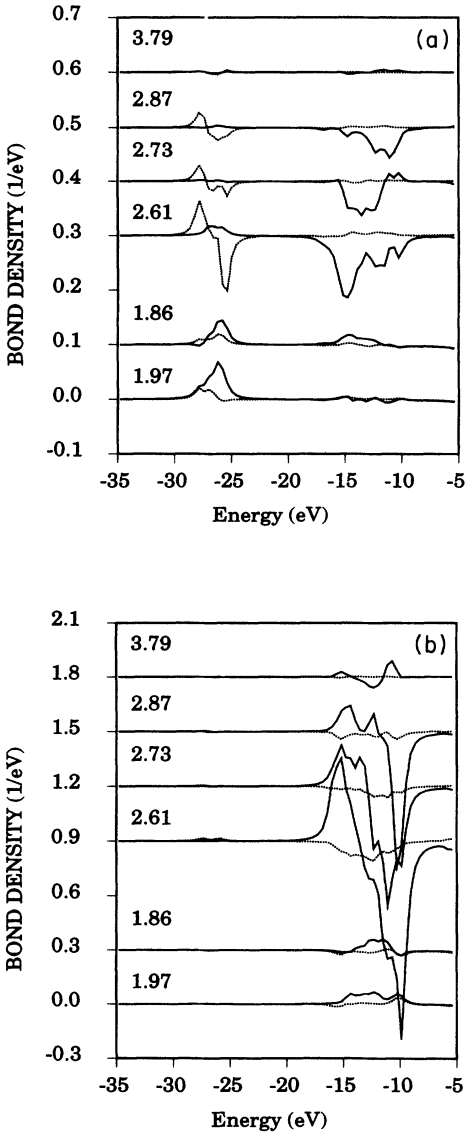

FIG. 5. Bond densities (a) between the seed O atoms $2s$ states and neighboring O $2s$, Al $3s$ (dotted curves), O $2p$, Al $3p$ (solid curves) states; (b) between the seed O atoms $2p$ states and the same states as in (a). Curves for atoms on different shells are shifted upward for a better view. From bottom upward, the first five groups of curves are for atoms label as 1, 4, 3, 5, 6 in Fig. 2(d). The top ones are for the O atoms 3.79 Å away from the seed O atoms and are beyond the cutoff radius of the cluster shown in Fig. 2(d). The bond lengths (Å) of the two atoms involved are printed on the top of their bond densities curves.

between the seed O $2s$, $2p$ states and the neighboring O $2s$, Al $3s$ (dotted curves), O $2p$, Al $3p$ (solid curves) states. From Fig. 5 we see that the features in the lower valence band and in the upper valence band are mainly due to the splitting of the bonding (positive bond density) and antibonding (negative bond density) 2s states and 2p states of the O-O bonds with bond lengths less than 3 Å. Around the main peak of the lower valence band at -26 eV, the O 2s states have weak covalent bonding with the nearest Al 3p states, since the value of their bond density shown in Fig. 5(a) is about 2% of the PDOS shown in Fig. 4. The corresponding bonding interaction with Al 3s and O 2p states is less than 1%. In the energy range from -14 eV to -10 eV within the upper valence band, the O 2p states have about 2% covalent bonding with the nearest Al 3p states, and 2% antibonding interaction with the 2s states of the O atom.

D. Charge density

From the definitions in Eqs. (17) and (26), the off-diagonal terms of the charge matrix are the integrals of all the corresponding bond densities over the occupied energy range. The bond densities shown in Fig. 5 indicate that the off-diagonal terms of the charge matrix are only about 2% of the diagonal terms given as the PDOS shown in Figs. 3 and 4. Thus the approximation used in Eq. (21) and the Mulliken charge analysis are valid. We listed in Table V the Mulliken orbital populations and charges of the seed Al, O atoms for the ten clusters studied. As in the case of the PDOS discussed in Sec. III C we see the same trends in the charge analysis.

To have a better picture of the charge distributions in bulk sapphire we plotted in Fig. 6 the valence charge-density contour diagrams on (a) the basal plane containing the three O atoms labeled as 1,2,3 in Fig. 1; (b) the cross-section plane formed by the O atom labeled as 2 and its two long bonded (3.72 a.u. or 1.97 Å) Al atoms shown in Fig. 1; (c) the cross section plane perpendicular to the above two planes and containing all the Al atoms shown in Fig. 1. Due to the reflection symmetry of the center of the unit cell shown in Fig. 1, only the lower half of the unit cell is covered in the charge-density contour diagrams shown in Fig. 6. The charge density of the whole crystal on these three planes can be easily produced by symmetry operations.

In Fig. 6(a), we see the charge accumulations along the nearest (4.76 a.u. or 2.52 Å) and the second nearest (4.93 a.u. or 2.61 Å) O-O bonds. In Fig. 6(b), the two Al atoms and the O atom on the right are on the plane, and are bonded through the long bond. The two O contours on the left are from the O atoms labeled as 4 and 5 in Fig. 1, which are 0.21 a.u. (0.11 Å) off the plane and bonded to the Al atoms through the short bond (3.51 a.u. or 1.86 Å). We see little difference in charge density between these two kinds of bonds, and there is no charge accumulation along the two Al-O bonds, indicating essentially ionic bonding. The dense and nearly spherical contours around 0.5 a.u. away from the Al nuclei are from the peaking in Al $3s3p$ orbitals. The Al $2s2p$ core orbitals

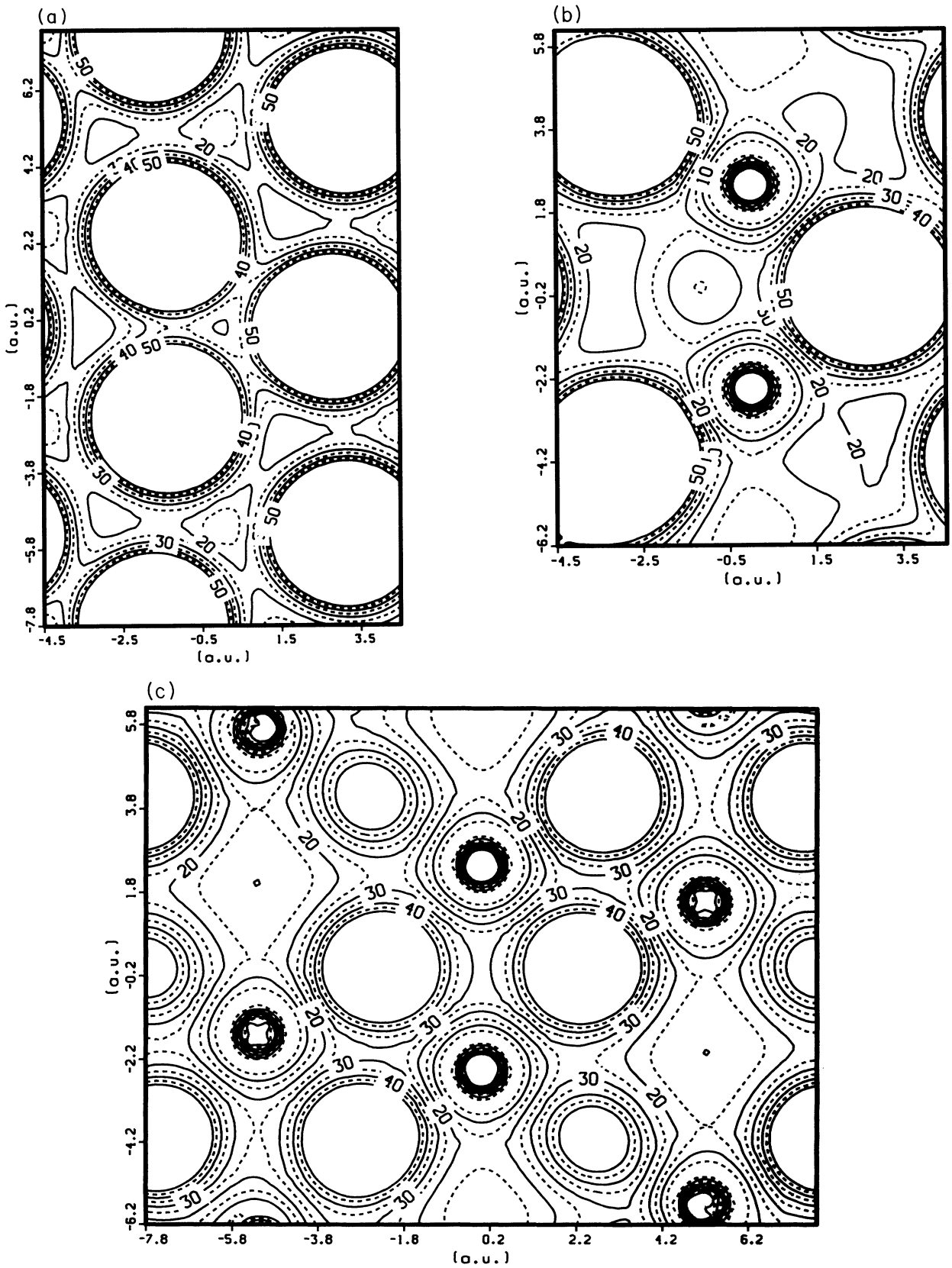

FIG. 6. The valence charge-density contour diagrams on (a) the basal plane containing the three O atoms labeled as 1,2,3 in Fig. 1; (b) the cross-section plane formed by the O atom labeled as 2 and its two long bonded (3.72 a.u. or 1.97 Å) Al atoms as shown in Fig. 1; (c) the cross-section plane perpendicular to the above two planes and containing all the Al atoms shown in Fig. 1. The minima and maxima contours are $0.005e/a_0^3$ and $0.050e/a_0^3$, and contour interval is $0.005e/a_0^3$.

TABLE V. The Mulliken orbital populations and charges Q (e) of the Al and O seed atoms for the ten clusters studied.

Type	O 2s	O 2p	Q_O	Al 3s	Al 3p	Q_{Al}
27 atom	1.90	5.90	-1.80	0.22	0.07	2.71
33 atom	1.99	5.89	-1.88	0.07	0.11	2.82
48 atom	1.99	5.93	-1.92	0.05	0.06	2.89
60 atom	2.00	5.91	-1.91	0.09	0.05	2.86
32 atom	1.94	5.91	-1.85	0.14	0.07	2.79
44 atom	2.00	5.94	-1.94	0.03	0.05	2.92
26 atom	2.00	5.94	-1.94	0.04	0.04	2.92
38 atom	2.00	5.90	-1.91	0.08	0.06	2.86
62 atom	2.00	5.96	-1.96	0.01	0.05	2.94
80 atom	2.00	5.95	-1.95	0.01	0.06	2.93

not shown here have peaks around 0.5 a.u. and then decay to zero exponentially. Therefore, we see a valley of low (valence) electron density ($< 0.005e/a_0^3$) within the shell from 0.6 a.u. to 1.0 a.u. from the center of the Al nucleus. From 1.0 a.u. on the density increases monotonically in the directions toward the nearest O atoms up to the cutoff density of $0.05e/a_0^3$.

In Fig. 6(c), all the Al atoms shown are on the plane, and all the O atoms are off the plane, the distances of which away from the plane can be estimated by the radii of the cutoff contour line. The two O contour lines near the center of the plot are from the two O atoms labeled as 1 and 3 in Fig. 1, which are 1.38 a.u. (0.73 Å) off the plane. We see that no charge accumulates between the Al atoms and the near-neighbor Al atoms. There exist two equivalent low charge-density ($0.005e/a_0^3$) cages of about 1.89 a.u. radius on the the upper left and lower right of the figure. The center of these two cages are the inversion centers of the sapphire crystal, one of which is the center of Fig. 1. These cages may serve as the interstitial sites for transition metal ions like Cr and Ti. Impurity cluster calculations are in progress and will be presented elsewhere.

In summary, the charge-density contour diagrams together with the density of states, bond density, and Mulliken charge analyses given in the preceding subsections indicate that the bulk sapphire has a highly ionic electronic structure, in accord with the earlier first-principles extended tight-binding calculations[23] and recent first-principles band-structure calculations.[7]

IV. CONCLUSIONS

In this paper, we have shown that the embedded-cluster method gives consistent results regardless the choice of different cluster centers, and provides all the major features of electronic structure for bulk sapphire with cluster size of 30 atoms, and reaches convergence in the results around 60 atoms. Our calculated density of states agree well with experiments and recent first-principle band-structure calculation, which give us the confidence on further surface and interface studies. Features in the valence density of states are interpreted with the help of the bond densities between the O atom and its near neighbors. Bulk sapphire is found to be mostly ionic, as indicated by the small ($\sim$ 2%) orbital overlaps between nearest-neighbor Al and O atoms and absence of charge accumulation in the bonding region.

ACKNOWLEDGMENTS

The work is supported by the U.S. Department of Energy (Division of Materials Science of the Office of Basic Energy Sciences) under Contract No. W-31-109-Eng-38 and by a grant of computer time on Cray computers at the National Energy Research Supercomputer Center. The work of D.E.E. was supported in part by Grant No. DE-FG02-84ER45097.

[1] S.-H Chou, J. Guo, and D. E. Ellis, Phys. Rev. B **34**, 12 (1986).
[2] W. Y. Ching, D. E. Ellis, and D. J. Lam, in *Phase Transitions in Condensed Systems: Experiments and Theory*, edited by D. Turnbull, G. S. Cargill, F. Spaepen, and K. N. Tu, MRS Symposia Proceedings No. 82 (Materials Research Society, Pittsburgh, 1987), p. 181.
[3] S. Xia, C. Guo, L. Lin, and D. E. Ellis, Phys. Rev. B **35**, 7671 (1987).
[4] P. K. Khowash and D. E. Ellis, Phys. Rev. B **39**, 1908 (1989).
[5] D. E. Ellis, J. Guo, and D. J. Lam, J. Am. Ceram. Soc. **73**, 3231 (1990).
[6] G. L. Goodman, D. E. Ellis, E. E. Alp, and L. Soderholm, J. Chem. Phys. **91**, 2983 (1989).
[7] Y. Xu and W. Y. Ching, Phys. Rev. B **42**, 4461 (1991).
[8] R. H. French, J. Am. Ceram. Soc. **73**, 477 (1990).
[9] V. A. Fomichev, Fiz. Tverd Tela (Leningrad) **8**, 2892 (1966) [Sov. Phys. Solid State **8**, 2312 (1967)].
[10] K. Codling and R. P. Madden, Phys. Rev. **167**, 587 (1968).

[11] E. T. Arakawa and M. W. Williams, J. Phys. Chem. Solids **19**, 735 (1968).
[12] A. Balzarotti, A. Bianconi, E. Burattini, M. Grandolfo, R. Habel, and M. Piacentini, Phys. Status Solidi B **63**, 77 (1974).
[13] A. Balzarotti, F. Antonangeli, R. Girlanda, and G. Martino, **29**, 5903 (1984).
[14] I. A. Brytov and Yu. N. Romashchenko, Fiz. Tverd. Tela (Leningrad) **20**, 664 (1978) [Sov. Phys. Solid State **20**, 384 (1978)].
[15] G. Dräger and J. A. Leiro, Phys. Rev. B **41**, 12919 (1990).
[16] C. G. Dodd and G. L. Glen, J. Appl. Phys. **39**, 5377 (1968); J. Am. Ceramic Soc. **53**, 322 (1970).
[17] D. W. Fischer, Adv. X-Ray Anal. **13**, 159 (1970).
[18] A. Balzarotti and A. Bianconi, Phys. Status Solidi B **76**, 689 (1976).
[19] S. P. Kowalczyk, F. R. McFeely, L. Ley, V. T. Gritsyna, and D. A. Shirley, Solid State Commun. **23**, 161 (1977).
[20] J. Olivier and R. Poirier, Surf. Sci. **105**, 347 (1981).
[21] J. A. Tossell, J. Phys. Chem. Solids **36**, 1273 (1975).
[22] R. A. Evarestov, A. N. Ermoshkin, and V. A. Lovchikov, Phys. Status. Solidi B **99**, 387 (1980).
[23] I. P. Batra, J. Phys. C **15**, 5399 (1982).
[24] S. Ciraci and I. P. Batra, Phys. Rev. B **28**, 982 (1983).
[25] R. W. G. Wyckoff, *Crystal Structures II*, 2nd ed. (Wiley, New York, 1964).
[26] E. J. Baerends, D. E. Ellis, and P. Ros, Chem. Phys. **2**, 41 (1973).
[27] A. Rosén, D. E. Ellis, H. Adachi, and F. W. Averill, J. Chem. Phys. **65**, 3629 (1976).
[28] D. E. Ellis, J. Guo, and H.-P. Cheng, J. Phys. Chem. **92**, 3024 (1988).
[29] D.E. Ellis, G. A. Benesh, and E. Byrom, J. Appl. Phys. **49**, 1543 (1978); Phys. Rev. B **20**, 1198 (1979).
[30] D. E. Ellis, G. A. Benesh, and E. Byrom, Phys. Rev. B **20**, 1198 (1979).
[31] B. W. Veal, D. E. Ellis, and D. J. Lam, Phys. Rev. B **32**, 5391 (1985).
[32] F. W. Kutzler, D. E. Ellis, D. J. Lam, B. W. Veal, A. P. Paulikas, A. T. Aldred and V. A. Gubanov, Phys. Rev. B **29**, 1008 (1984).
[33] D. E. Ellis, Int. J. Quan. Chem. **2**, 35 (1968).
[34] D. E. Ellis and G. S. Painter, Phys. Rev. B **2**, 2887 (1970); in *Computational Methods in Band Theory*, edited by P. M. Marcus, J. F. Janak, and A. R. Williams (Plenum, New York, 1971), p. 271.
[35] G. S. Painter and D. E. Ellis in *Computational Methods in Band Theory*, edited by P. M. Marcus, J. F. Janak, and A. R. Williams (Plenum, New York, 1971), p. 276.
[36] P. P. Ewald, Ann. Phys. (N.Y.) **64**, 253 (1921).
[37] M. P. Tosi, *Solid State Physics*, edited by H. Ehrenreinch, F. Seitz, and D. Turnbull (Academic, New York, 1964), p. 107.
[38] W. Kohn and L. J. Sham, Phys. Rev. **140**, A1133 (1965).
[39] U. von Barth and L. Hedin, J. Phys. C **5**, 1629 (1972).
[40] O. Gunnarsson and B. I. Lundqvist, Phys. Rev. B **13**, 4274 (1976).
[41] J. P. Perdew and A. Zunger, Phys. Rev. B **23**, 5048 (1980).
[42] J. C. Slater, Phys. Rev. **81**, 385 (1951).
[43] D. C. Langreth and M. J. Mehl, Phys. Rev. Lett. **47**, 446 (1981).
[44] D. C. Langreth and M. J. Mehl, Phys. Rev. B **28**, 1809 (1983).
[45] C. D. Hu and D. C. Langreth, Phys. Rev. B **33**, 943 (1986).
[46] J. P. Perdew and W. Yue, Phys. Rev. B **33**, 8800 (1986); *ibid.* **33**, 8822 (1986).
[47] C. Lee, W. Yang, and R. G. Parr, Phys. Rev. B **37**, 785 (1988).
[48] M. Norman and D. D. Koelling, Phys. Rev. B **28**, 4357 (1983).
[49] F. W. Kutzler and G. S. Painter, Phys. Rev. Lett. **59**, 1285 (1987); Phys. Rev. B **37**, 2850 (1988).
[50] R. S. Mulliken, J. Chem. Phys. **23**, 1833 (1955); **23**, 1841 (1955).
[51] J. Guo, D. E. Ellis, G. L. Goodman, E. E. Alp, L. Soderholm, and G. K. Shenoy, Phys. Rev. B **41**, 82 (1990).
[52] J. Guo, D. E. Ellis, E. E. Alp, and G. L. Goodman, Phys. Rev. B **42**, 251 (1990).

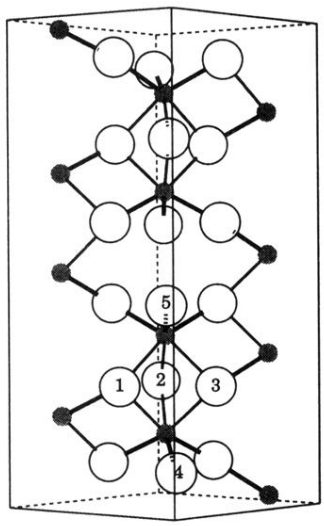

FIG. 1. A perspective view of the hexagonal unit cell of sapphire. The filled circles label Al atoms, and open circles O atoms. The dark thick lines label the short Al-O bonds (1.86 Å), the light thin lines the long Al-O bonds (1.97 Å).

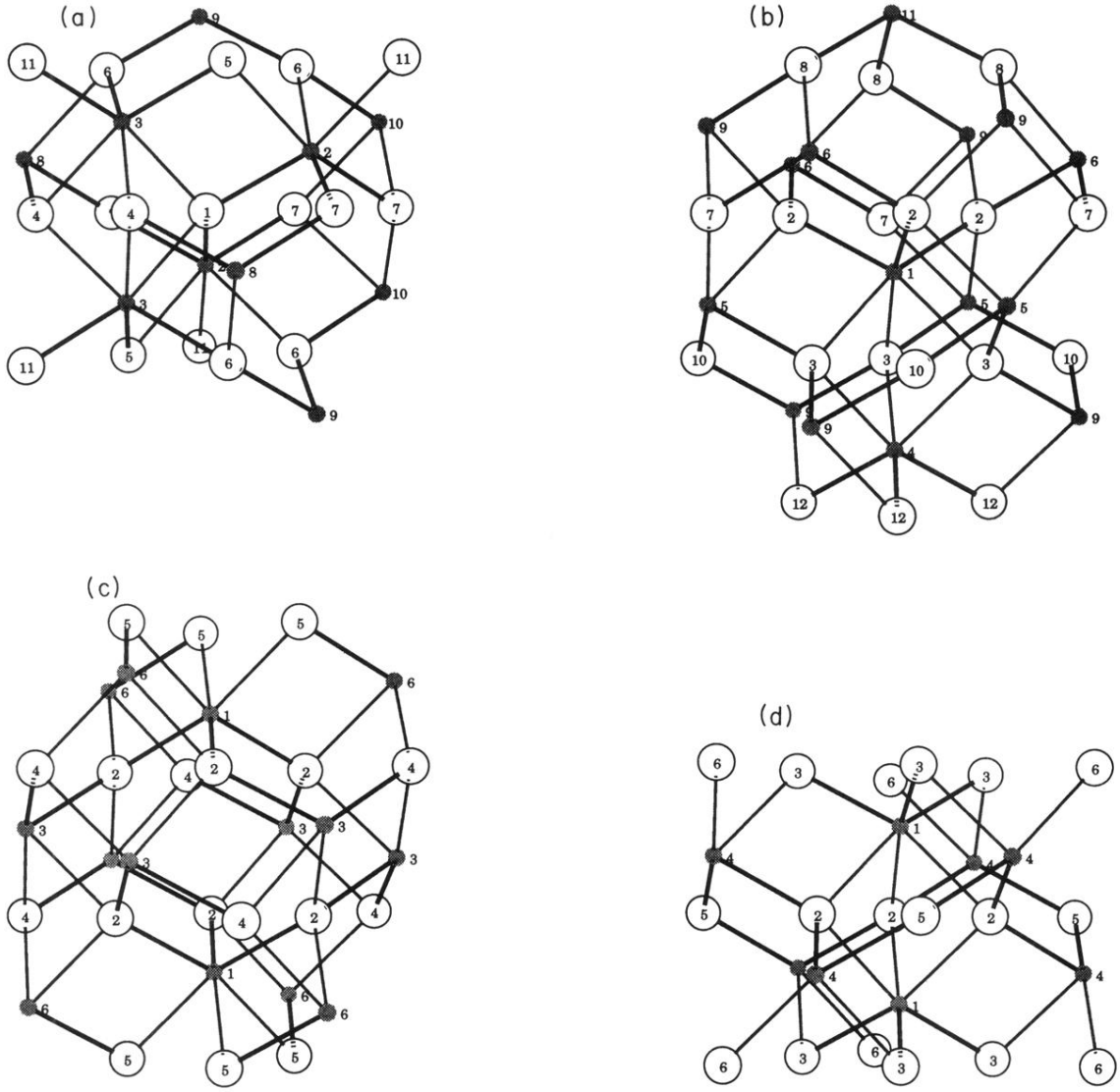

FIG. 2. Perspective views of the four clusters chosen in the calculations. (a) 27-atom cluster of C_2 symmetry; (b) 33-atom cluster of C_3 symmetry; (c) 32-atom cluster of S_6 symmetry; (d) 26-atom cluster of D_3 symmetry. The numbers label the different shells of atoms in the ascending order according to their distances from the center. Same conventions as Fig. 1.